

Interhemispheric Asymmetries in Magnetospheric Energy Input

Eftyhia Zesta,¹ Athanasios Boudouridis,² James M. Weygand,³ Endawoke Yizengaw,⁴
Mark B. Moldwin,⁵ and Peter Chi⁶

ABSTRACT

Energy transfer from the solar wind to the magnetosphere-ionosphere-thermosphere system occurs via multiple routes with coupling efficiency depending on the Interplanetary Magnetic Field (IMF), solar wind, and the magnetosphere prior state. The energy is not always released in the two hemispheres symmetrically. Ultra low frequency (ULF) waves are the natural perturbations of the magnetosphere and the plasma in it, thus constituting an excellent diagnostic of how energy is transported throughout this complex system. We explore the question of how energy is deposited asymmetrically in the two hemispheres by studying (1) asymmetries of auroral currents and (2) asymmetries in ULF wave power at magnetically conjugate locations. We also construct a Southern Hemisphere auroral electrojet (AE) index and compare it with the standard AE index. We find that while in general the north and south electrojet indices correlate well, significant asymmetries occur frequently, primarily in the local midnight region. We also find that at low latitudes and midlatitudes the north-to-south wave-power ratio exhibits clear annual variation with a systematic offset: the Northern Hemisphere always has stronger power than the Southern Hemisphere. This systematic asymmetry is also seen in the ionospheric total electron content (TEC), implying a close link.

Key Points:

Interhemispheric asymmetries in ULF wave power and total electron content
A southern auroral electrojet index and comparison with the standard AE index
Interhemispheric asymmetries between northern and southern auroral electrojet indices

Key Terms: equatorial ionosphere, equatorial electrojet (EEJ), ground-induced currents (GIC)

¹Heliophysics Science Division, NASA Goddard Space Flight Center, Greenbelt, Maryland, USA

²Center for Space Plasma Physics, Space Science Institute, Boulder, Colorado, USA

³Institute of Geophysics and Planetary Physics, University of California, Los Angeles, Los Angeles, California, USA

⁴Institute for Scientific Research, Boston College, Chestnut Hill, Massachusetts, USA

⁵Atmospheric, Oceanic, and Space Science (AOSS), University of Michigan, Ann Arbor, Michigan, USA

⁶Department of Earth and Space Sciences, University of California, Los Angeles, Los Angeles, California, USA

1.1. INTRODUCTION

It is generally assumed that most of the dynamic geospace phenomena, like magnetic storms and substorms, develop in unison in both Northern and Southern Hemispheres, typically starting in the polar regions. High-latitude geomagnetic field lines carry a load of field-aligned currents (FACs) and electromagnetic waves directly from the magnetopause, where the heavy coupling from the solar wind to the magnetosphere occurs, down to the ionosphere and thermosphere, depositing energy in the form

of Poynting flux that heats both the ionosphere and neutral atmosphere. A part of the solar-wind energy gets processed in the magnetotail first, and is ultimately deposited in the ionosphere via both currents and electromagnetic waves, but also particle precipitation that can form bright auroras. Another part of the solar-wind energy is stored in the inner magnetosphere and couples to the mid-latitude and low-latitude ionosphere through electric fields, waves, and particle precipitation. During equinox, it is generally assumed that the load of currents and waves is approximately symmetric into the north and south polar ionospheres, but becomes quite asymmetric when either of the poles is tilted toward the Sun during the solstices [e.g., *Wu et al.*, 1991]. At those times, the uneven solar EUV illumination becomes a controlling factor for the asymmetric ionospheric conductivity in the two polar regions, leading to large asymmetries in the electrodynamic coupling with the magnetosphere and the amount of heating that is transferred to the neutrals.

While seasonal effects are strong drivers of interhemispheric asymmetries, other factors, such as the dipole tilt with respect to the rotation axis, the Interplanetary Magnetic Field (IMF) orientation, local magnetic field structures, and even atmospheric dynamics, can and do play a significant role in the strong interhemispheric asymmetries that are observed at all latitudes. For example, *Knipp et al.* [2000] showed significant difference in the amount of energy input, both from Joule heating and precipitation, in the two hemispheres during an 11-hr interval in May 1999. *Knipp et al.* argued that the large asymmetries were due to both the Northern Hemisphere sunward tilt and to the IMF orientation.

The tilt and offset of the dipolar part of the Earth's magnetic field places the polar caps at different geographic latitudes resulting in lower geomagnetic latitudes seeing 24 hr darkness in the Southern Hemisphere in the Americas longitude sector than in the Northern Hemisphere during northern summer, further exacerbating conductivity and electrodynamic asymmetries. *Cnossen and Richmond* [2012] demonstrated via modeling that the tilt angle of the geomagnetic dipole is a strong controlling factor in the distribution of Joule heating in the high latitudes and in the neutral temperature and winds. *Förster and Cnossen* [2013] took this work further to demonstrate, again via modeling, the effect the nondipolar components of the Earth's magnetic field have in interhemispheric asymmetries. They found that while the effect in the large-scale plasma convection was rather small, the effect on the neutral winds was substantial.

It is a common assumption, particularly in simulations, that auroral activity, brightenings, and dynamics in the Northern and Southern hemispheres are a mirror image of each other, based on the assumption that the magnetospheric processes are similarly mapped down to the two

polar regions, and the source particles are evenly distributed along the same field lines to the two ionospheres. While seasonal differences have been statistically reported [e.g., *Newell et al.*, 1996; *Liou et al.*, 2001], the global patterns of precipitation are typically assumed symmetric in the two hemispheres.

The substorm phenomenon is perhaps the most common and dramatic nightside auroral intensification. All of today's models of substorms are based mostly on Northern Hemisphere observations and assume conjugacy between hemispheres. Studies of the conjugacy (or not) of substorm onset and its dynamics have primarily relied on ground or aircraft imagers and magnetometers located at conjugate points [e.g., *Belon et al.*, 1969; *Stenbaek-Nielsen et al.*, 1972, 1973; *Hajkowicz*, 2006; *Motoba et al.*, 2014]. Studies based on older instrumentation and limited cases found good conjugacy between of the auroras for both quiet and active conditions [e.g., *Belon et al.*, 1969; *Stenbaek-Nielsen et al.*, 1972], but new studies with more sophisticated instrumentation and longer statistical studies have begun to demonstrate interhemispheric asymmetries in larger and smaller scale size structures [e.g., *Hajkowicz*, 2006; *Laundal and Østgaard*, 2009; *Motoba et al.*, 2014; *Weygand et al.*, 2014a]. Fewer studies were able to use satellite auroral imagery on few fortuitous conjunctions [*Ostgaard et al.*, 2004, 2007; *Frank and Sigwarth*, 2003; *Sato et al.*, 2012]. Many of these studies have reported significant asymmetries, both in the location and timing of the substorm onset [e.g., *Morioka et al.*, 2011; *Sato et al.*, 1998; *Weygand et al.*, 2014b]. *Kivelson et al.* [1996] and *Ostgaard et al.* [2004, 2007] found that the north-south displacement of the onset systematically depends on the IMF B_y sign and magnitude.

Frank and Sigwarth [2003] presented the first simultaneous satellite observations of a substorm onset (observed by Polar VIS camera at both hemispheres simultaneously). They found a 1–2 min delay in the occurrence of the onset between the two hemispheres and that traditional mapping would place the source of the onset from the two hemispheres on significantly different locations on the tail. Clearly, our understanding of how tail dynamics couple down to the ionosphere is incomplete.

While there are many works looking at the asymmetries of substorm auroral dynamics, there are limited studies that demonstrate asymmetric auroral features and energy input for less active periods. *Shi et al.* [2012] showed that the cusp location moved asymmetrically between the two hemispheres while the dipole tilt angle increased, resulting at the cusp forming at different latitudes at the two hemispheres. *Fillingim et al.* [2005] used coincidental observations from IMAGE FUV and Polar UVI and observed significant asymmetries in the structure of the afternoon aurora, which they attributed to IMF B_y effects. *Stubbs et al.* [2005] looked at the relative location

of the complete auroral oval from simultaneous IMAGE and Polar observations from both hemispheres and found that not only IMF B_y , but also B_x , affect the displacement of the oval in the two hemispheres. *Motoba et al.* [2012] recently analyzed detailed observations of auroral beads from conjugate all-sky auroral imagers that occurred ~ 15 min before a substorm onset. They found that the beads developed simultaneously and with great similarity in the two hemispheres.

There is evidence that the auroral electrojets exhibit seasonal asymmetries [*Wu et al.*, 1991], although most studies depend on spatially limited magnetometer chains, or individual conjugate pairs of magnetometers. *Wu et al.* [1991] reported that the substorm westward electrojet flows at higher latitudes in the winter hemisphere than in the summer hemisphere by as much as 4° . The interhemispheric asymmetries of the auroral electrojets are likely a direct result of the interhemispheric asymmetries in field-aligned currents (FACs). Theoretical studies have predicted that conductivity differences between the winter and summer hemispheres will create a set of interhemispheric FACs (IHCs) [*Benkevich et al.*, 2000]. The IHCs flow from one hemisphere to the other along highly conductive magnetic field lines connecting the two conjugate auroral zones and have the effect of redistributing the ionospheric currents in the two hemispheres with significantly different conductivities. Although IHCs have been modeled from first principles [*Benkevich et al.*, 2000; *Lyatskaya et al.*, 2014a; 2014b], they have yet to be observed, primarily due to lack of the necessary observations, that is, coincidental observations of FACs from both hemispheres on the same local time sector. Our lack of conjugate observations on the global scale has clearly limited our understanding of dynamic phenomena like substorms.

This is where more recent data assembly techniques like AMPERE [*Anderson et al.*, 2002] and SuperMAG [*Gjerloev*, 2012] can help break through the prior observational limitation. The Active Magnetosphere and Planetary Electrodynamics Response Experiment (AMPERE) Science Data Center is a facility that uses magnetometer data from the 66 IRIDIUM satellites and sophisticated algorithms to provide the global FAC patterns every 10 min [*Anderson et al.*, 2002]. SuperMAG [*Gjerloev*, 2012] is a worldwide collaboration of ground magnetometer chains that operate more than 300 magnetometers and provides easy access to validated ground magnetic field perturbations in the same coordinate system and identical time resolution with a common baseline removal approach. Products like the global equivalent ionospheric currents are also provided. It is now possible to support large-scale interhemispheric studies.

Here we focus on two specific topics. First, in Section 1.2, we discuss interhemispheric asymmetries of

the auroral electrojets as a means of understanding how dynamic phenomena develop differently in the two hemispheres. Then, in Section 1.3, we discuss interhemispheric asymmetries of the power of ultra low frequency (ULF) waves at low latitudes and midlatitudes and see what the role of the ionosphere is in such asymmetries. We end with a brief summary.

1.2. ASYMMETRIES IN HIGH-LATITUDE DYNAMICS AND THE AURORAL CURRENTS

The auroral electrojet (AE) index (*Davis and Sugiura*, 1966) is traditionally calculated from a set of 10–13 ground magnetometer stations located around the typical northern auroral oval location (between 60° and 70° geomagnetic latitude). There is no Southern Hemisphere AE index because there is not sufficient station coverage from the southern auroral oval. The AE index is used as the most common indicator of global geomagnetic activity and it is well correlated with the strength of the auroral electrojets and also with auroral activity. It is typically used for identifying the occurrence, onset, and strength of a substorm. Considering the evidence for significant differences in both the location and timing of the auroral substorm onset and dynamics, it follows that the AE index should exhibit similar asymmetries.

Efforts to calculate a southern AE index are few, given the limited landmass availability at the appropriate latitudes in the Southern Hemisphere. *MacLennan et al.* [1991] used 22 available ground magnetometer stations from Antarctica to calculate a southern AE (SAE) index for 7 days in June 1982 and compare it with the northern World Data Center (WDC) AE. They found that the WDC AE was consistently stronger than the SAE index, which was likely due to seasonal effects. The *MacLennan et al.* [1991] study, however, included stations within a wide latitude range, from 50° to 90° magnetic, thus almost certainly including stations that at any moment were not within the auroral oval. Similarly, *Saroso et al.* [1992] compared the WDC AE with a southern polar cap index SAE, derived from four evenly spaced Antarctic magnetometer stations. The comparison results from this study are inconclusive, mostly because the southern stations were at higher magnetic latitude than the AE stations.

1.2.1. AE Interhemispheric Asymmetries

Recently, *Weygand and Zesta* [2008] conducted a study similar to that of *MacLennan et al.* [1991] and created an SAE index for comparison with the World Data Center (WDC) AE index for 7 days in December 2005. *Weygand and Zesta* [2008] used all seven available Southern Hemisphere stations at magnetic latitudes between -60° and -71° , so that both northern and southern stations

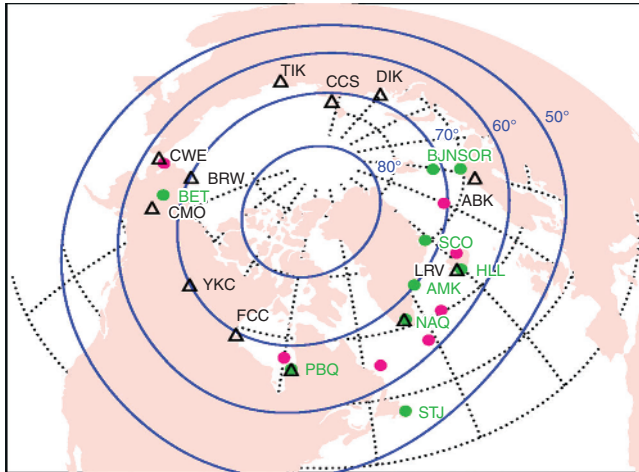


Figure 1.1 Map of northern and southern stations used for NAE and SAE calculations in *Weygand and Zesta* [2008]. In magenta are the north conjugate locations of the 7 southern stations for SAE, in green are the 9 northern stations for NAE, and the black triangles are the 12 standard AE stations.

were within the same topological region of the magnetosphere at the same time.

Figure 1.1 is a reproduction of Figure 2 from *Weygand and Zesta* [2008] and displays the location and distribution of all the Northern and Southern (projected to the north) hemisphere stations used for their study. The black triangles depict the standard AE stations, magenta solid circles are the north conjugate locations for the seven southern stations, as projected by the International Geomagnetic Reference Field (IGRF) model, and the green solid circles are northern stations selected for being as near conjugate as possible to the seven southern stations and are used to produce a northern AE (NAE) index conjugate to SAE. Black dotted lines are lines of geographic latitude and longitude and the solid blue lines are lines of constant geomagnetic latitude, calculated from Altitude Adjusted Corrected Geomagnetic Coordinate model [Baker and Wing, 1989]. The southern stations MAW, SYO, SNA, NVL, HBA, and WSD provide closely spaced coverage of a good portion of the auroral zone while MCQ station is farther away leaving a gap between WSD and MCQ and an even bigger gap from MCQ to MAW. The lack of similar coverage from the seven southern stations and the WDC AE stations is why *Weygand and Zesta* [2008] also created the conjugate NAE index from nine northern stations. There are more northern magnetometer stations than southern stations because exact conjugate stations are not always available. So, where necessary, data from the northern magnetometers that “surround” the conjugate southern station location are averaged together. For example, the conjugate signature for HBA (magenta circle immediately to the right of

PBQ) is produced by averaging the data from NAQ, STJ, and PBQ. All the details of the different stations used and their coordinates are given in the original paper.

Figure 1.2 is reproduced from Figures 4 and 9 of *Weygand and Zesta* [2008] and shows the calculated indices for 10 December 2005 (an active day) on the top, and for 8 December 2005 (a quiet day) on the bottom. For each day, the AU, AL, and AE indices for the southern (SAE/AU/AL), conjugate Northern Hemisphere data (NAE/AU/AL), and the WDC indices are shown. The Northern Hemisphere indices are given in the top panels as solid black lines, and the Southern Hemisphere indices are shown in the bottom panels, also in solid black lines. The gray lines in the top panels are the WDC quick look indices that can stand in place of the standard AE, AU, and AL indices. In Figure 1.2a, only the first 12 hr of the day are available for 10 December 2005. There is good agreement between the northern indices and the WDC indices for the substorm just after 0600 UT visible in both NAE and AE. The correlation coefficient between AE and NAE is 0.86, which implies that activity is happening in local times where there is good coverage from southern stations (since the conjugate locations to the southern index are reproducing well the standard AE index) and the large gaps in coverage are not affecting this particular day. However, there is less agreement between the NAE and SAE indices, with a correlation coefficient of 0.69, which implies some real asymmetries between the Northern and Southern Hemispheres. The NAE and AE have clearly greater magnitude perturbations than the southern index, even though the event occurs during northern winter (low conductivity) and southern summer (high conductivity), when we expect stronger ionospheric currents in the Southern Hemisphere. The evidence therefore indicates the existence of significant asymmetries between the Northern and Southern hemisphere auroral electrojets, seemingly unrelated to seasonal variations and strong enough to overcome the expected seasonal asymmetries.

Figure 1.2b shows the northern and southern indices in the same format as in the previous event for a quiet day, 8 December 2005, and therefore the magnitude of the indices is significantly smaller. The black bar in each panel indicates the period of time when there is no station coverage in the local midnight sector for either SAE or NAE. For this event, there are significant differences between NAE and AE, particularly between 18 and 24 UT. In fact, the SAE index correlates much better with AE at that period of time, picking up the substorm activity at ~20 UT that is totally missed by NAE. Even for this very quiet day, there is strong evidence for interhemispheric asymmetries, likely due to IMF B_y .

It is likely that the interhemispheric currents, which have been theoretically postulated [Benkevich *et al.*, 2000; Lyatskaya *et al.*, 2014a, 2014b], contribute greatly to the

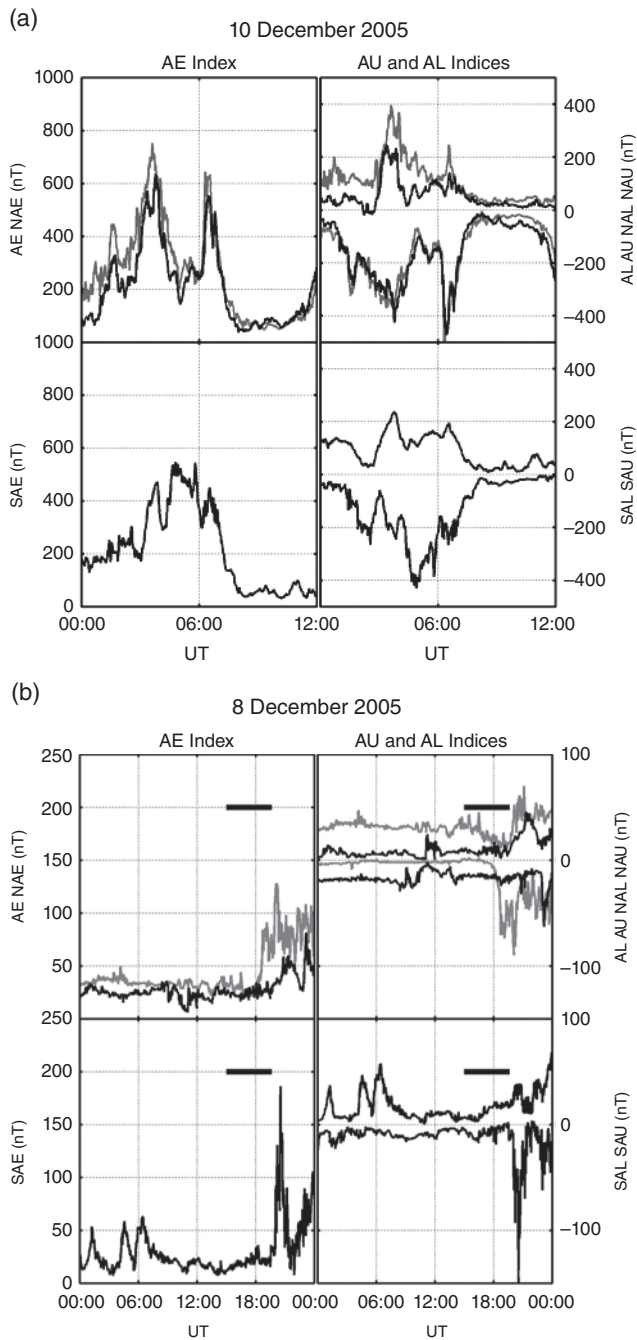


Figure 1.2 AE, NAE, and SAE calculations for (a) the active day on 10 December 2005, and (b) the quiet day on 8 December 2005. The black lines in top and bottom panels are the NAE/NAU/NAL and SAE/SAU/SAL indices, respectively, while the gray lines on the top panels are the standard AE/AU/AL indices.

observed asymmetries. *Weygand and Zesta* [2008] showed that the maximum north-south magnitude differences in the ground magnetic perturbations are seen in the local midnight region and are likely due to interhemispheric asymmetries of the nightside westward electrojet. By extension, they suggested that when the local midnight region is well

covered by stations in Antarctica, then the NAE can reasonably represent the WDC AE and then differences between NAE and SAE reasonably represent interhemispheric asymmetries in the auroral electrojets. This now opens the way for significant advancement in interhemispheric studies and in the effects of such asymmetries in global simulations.

Weygand et al. [2014a] expanded on the work of *Weygand and Zesta* [2008] by conducting a large statistical study on the correlation between the SAE, NAE, and AE indices. *Weygand et al.* [2014a] used the most complete, to date, database of Southern Hemisphere auroral magnetometers from 2005 to 2010 and were able to calculate the NAE and SAE indices simultaneously for a total of 274 days. (The individual NAE and SAE indices were available for a significantly greater number of days in each case.). The station distribution used in *Weygand et al.* [2014a] is very similar to that of Figure 1.1 with some small changes.

Figures 1.3a and b are reproduced from Figures 10 and 12 of *Weygand et al.* [2014a] and demonstrate some fundamental statistical properties for the northern and southern indices, based on the 274 days of available observations. Figure 1.3a shows histograms of the daily correlation between the SAE and NAE indices (top panel) and their mean daily differences (bottom panel). The correlation distribution peaks at 0.8, but the mean of the distribution is 0.65 with a maximum of 0.98 and a minimum of -0.2 . This implies that, statistically, Northern and Southern Hemispheres electrojets are well correlated in terms of the timing of their dynamic changes. However, since the distribution is widely spread, there are often times of significant interhemispheric asymmetries. *Weygand et al.* [2014a] showed that the highest correlations occur during spring and to a lesser degree at fall, while the lowest correlations occur during northern winter and summer, when the two hemispheres are very asymmetrically illuminated, so there is an observed seasonal effect. The low correlation values in the top panel of Figure 1.3a correspond to quiet geomagnetic activity, as was also shown by *Weygand and Zesta* [2008], because the linear correlation of a nearly flat line (no activity) with another flat line is nearly zero by definition. This is demonstrated more clearly in Figure 1.3b where the mean daily correlation coefficients between SAE-NAE and SAE-AE are plotted with respect to the daily mean of the SAE index on the top and bottom panels, respectively. The black dots are the individual daily means and the gray squares are means of SAE index bins for a bin size of 50 nT. The gray bars are the standard deviation of the means for each bin. The gray line is drawn as visual aid for the data trends. Low correlation coefficients are only associated with very low geomagnetic activity, while higher correlations exist for both quiet and active days. Highly active days have only higher correlation coefficients, >0.5 .

The persistent magnitude difference between SAE and NAE indices demonstrated in Figure 1.3a, bottom panel,

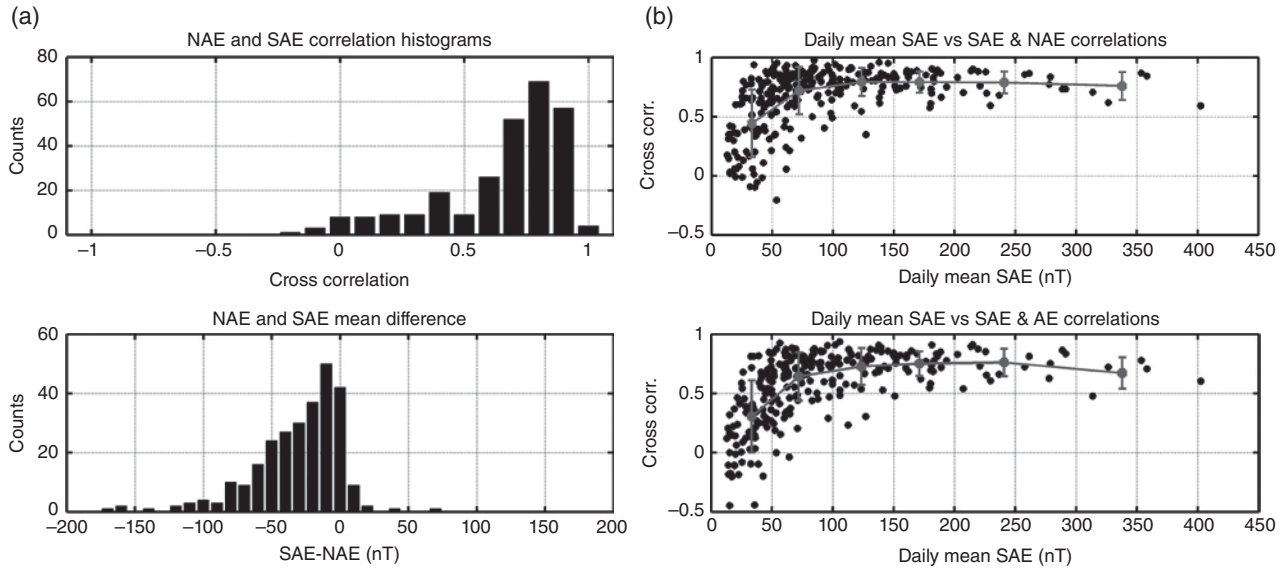


Figure 1.3 (a) Histograms of the SAE-NAE daily correlations (top) and of the SAE-NAE mean daily differences (bottom); (b) daily mean SAE-NAE correlation (top) and SAE-AE correlations (bottom) with respect to the daily mean SAE [from Weygand *et al.*, 2014a].

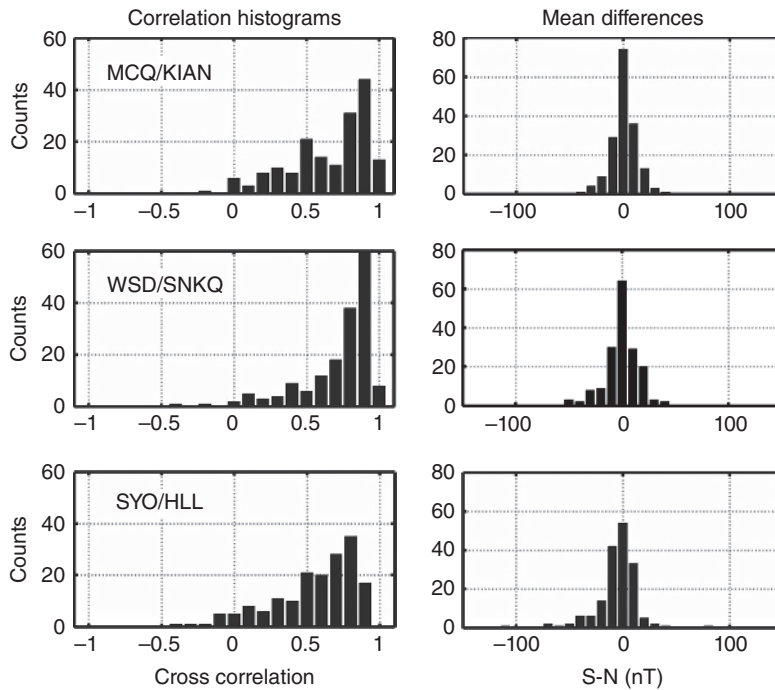


Figure 1.4 (Left) Histograms of the correlations between closely conjugate south-north pairs of stations MCQ-KIAN, WSD-SNKQ, and SYO-HLL, and (right) histograms of the difference between the H component for each pair of stations.

with SAE on average smaller than NAE was reported also by Maclellan *et al.* [1991] and seems to indicate that the northern auroral electrojets are consistently stronger than the southern auroral electrojets. Since this is not a physically intuitive result, Weygand *et al.* [2014a] explored this matter further by isolating north-south pairs of

stations included in the SAE and NAE calculations with good and poor conjugacy.

Figure 1.4 is a reproduction of Figure 14 from Weygand *et al.* [2014a] and shows, on the left column, histograms of the daily correlation of the H magnetic field component for station pairs MCQ-KIAN, WSD-SNKQ, and SYO-HLL,

where the first part of each pair is a southern station and the second is the northern station. On the right column of Figure 1.4, the daily mean differences are shown for the same three pairs of stations. The correlation plots for all three pairs are very similar to the SAE-NAE correlation histogram shown in Figure 1.3a (top panel), with the correlations peaking at 0.9. However, the daily mean histograms for the three pairs in Figure 1.4 are significantly different from the SAE-NAE daily mean in Figure 1.3a, bottom panel. The mean daily difference for the three conjugate pairs is centered at 0 nT. Even though there is a spread to the distribution and there are clearly times with large interhemispheric asymmetries, the histograms of Figure 1.4, right column, seems to indicate that there is no systematic asymmetry between the north and south electrojets. The distributions of Figure 1.4 were produced with daily averaged values of north-south amplitude differences and for all different conditions. In Figure 1.5, we plot histogram distributions of the amplitude differences for the same three pairs of closely conjugate stations, but for 1 min averaged differences observed only in the local midnight region, ± 3 hr around 00 MLT. The differences between north and south responses to the electrojet for low K_p are similar to those in Figure 1.4, namely centered around 0 and denoting no obvious systematic asymmetry between Northern and Southern Hemispheres. The histograms for high K_p values, however, show that for two of the three pairs, MCQ/KIAN and SYO/HLL, the peak is negative, indicating persistent stronger amplitudes at the northern

stations. The third pair, WSD/SNKQ, has stations located in significantly different geographic latitudes.

The electrojet indices (AE, SAE, or NAE) are sensitive to the global DP2 current system, namely the global-scale two-cell convection pattern [Nishida, 1968], but are also most strongly sensitive to the nightside westward electrojet that is typically the result of substorm or other strong activity, known as the DP1 current system [Nishida, 1968]. One then would expect most of the interhemispheric asymmetries in the north and south indices to also be strongly sensitive to the nightside westward electrojet.

Figure 1.6 is a reproduction of Figure 17 from Weygand *et al.* [2014a] and demonstrates exactly this point. Figure 1.6 shows a superposed epoch analysis of the SAE-NAE differences on the top panel, and the difference in the H component between the south and north stations of the closely conjugate pairs that were discussed in Figure 1.4 and from all available data in the bottom three panels. For each pair of stations, the black line is the median and the two gray curves are the upper and lower quartiles of the distribution. The open circle in each panel indicates local midnight and the solid circle indicates local noon for that pair of stations. While the median curve varies minimally, it is clear from the quartile curves that the largest differences between the north and south stations of the pair occur around local midnight and are therefore associated with the nightside westward electrojet. We therefore propose that for times when there is good coverage of the local midnight region from the

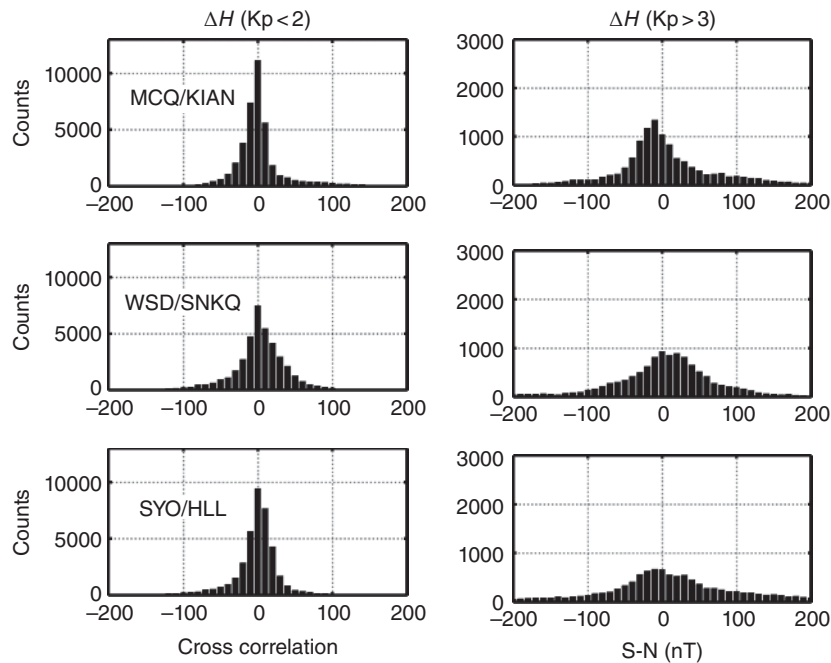


Figure 1.5 Histograms of the H component differences for the same three pairs of closely conjugate stations as in Figure 1.4. On the left are the histograms for low geomagnetic activity ($K_p < 2$) and on the right are the histograms for high geomagnetic activity ($K_p > 3$).

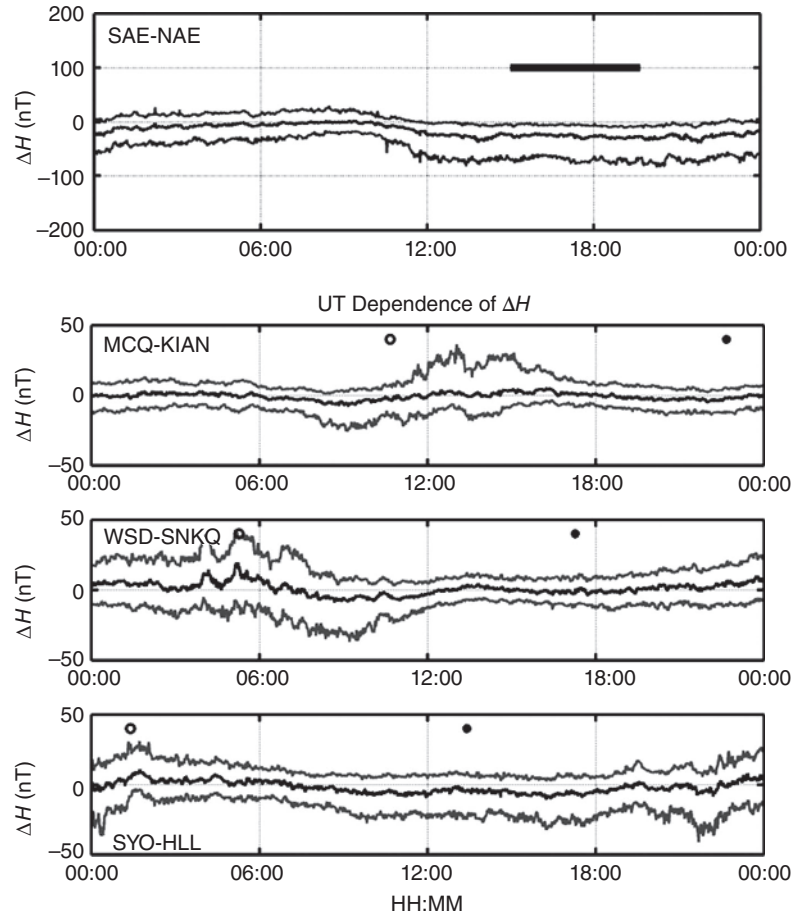


Figure 1.6 (Top panel) Superposed epoch UT dependence of the SAE-NAE differences, solid line. The lighter shade lines are the upper and lower quartiles of the distribution. (Panels 2–4) Superposed epoch of the difference in the H component for the same three closely conjugate pairs of ground magnetometer stations of Figure 1.4. The station pairs are given on the left side of the panel; the open circles indicate local midnight for each station, and the filled circles indicate local noon. Upper and lower distribution quartiles are shown in lighter shade lines around the main distribution.

Southern Hemisphere, the SAE can be used as the equivalent Southern Hemisphere Auroral Electrojet index.

Most important, Figure 1.6, in combination with the histograms of Figure 1.5, gives an insight into possible reasons for the systematic asymmetry between SAE and NAE from Figure 1.3a. The negative SAE-NAE distribution peak is manifested in the 12–24 UT period, which engulfs the time period when no southern stations are in near local midnight (indicated by the horizontal bar), where most of the amplitude and differences in SAE and NAE originate. The longitudinal distribution of stations is clearly a contributor to the observed systematic asymmetry between SAE and NAE. The UT differences of the H component for the three pairs in Figure 1.6 demonstrate another important point. While the daily averaged differences may be centered at 0 (Fig. 1.4), the distributions can be systematically positive or negative during the day. This and the systematic differences

for higher geomagnetic activity in Figure 1.5 indicate that the SAE/NAE systematic asymmetry is not due just to the longitudinal gaps in the Southern Hemisphere, but also to other factors like the geographic differences between station pairs, interhemispheric currents, or activity levels.

While the precise causes of the observed north-south asymmetry in SAE and NAE remain unclear, the spread of the histogram distributions in Figures 1.4 and 1.5 demonstrate the significant interhemispheric asymmetries that habitually occur.

1.2.2. The Effect of Solar Wind and IMF on the Interhemispheric Asymmetries

We now look at the role the solar wind and IMF may play in the observed interhemispheric asymmetries as evidenced by the calculated SAE and NAE indices.

Specifically, we examine how different solar-wind parameters affect the correlation between the SAE and NAE indices.

For the solar-wind study, we recalculated cross correlation coefficients between the three AE indices (standard AE, NAE, and SAE) at a much faster cadence than was used in the *Weygand et al.* [2014a] work. We used our complete database, which amounts to 274 days, from December 2005 to August 2010, when all three indices are available. The cross correlation coefficients are estimated every 10min with a correlation window of 2hr around each point in time. The solar-wind and IMF quantities are taken from ACE data and are propagated to $17 R_E$ using the Weimer technique [*Weimer et al.*, 2003; *Weimer*, 2004]. In order to include propagation to the ionosphere and effects of preconditioning of the magnetosphere by previous solar wind and IMF values, we introduce two additional time constants: delay time, T_d , for the propagation to the ionosphere from $17 R_E$, and preconditioning time, T_p , for averaging the solar wind and IMF data before each point. For T_d we use 10min as an average propagation window from $17 R_E$ upstream to the ionosphere. For T_p we use 20min and that is the time period beyond the 10min (T_d) for which we average the SW parameters to get a sense of preconditioning. Therefore, each index correlation is assigned solar wind and IMF values by shifting the propagated ACE data by T_d minutes, and then averaging the solar-wind data for T_p minutes before that. With all the correlation coefficients calculated, a statistical study of the effects of solar wind and IMF conditions on the electrojet index correlations can be performed. While a more complete and focused manuscript is in preparation, we show here some key

results of this new work. Specifically, we examine the effect of IMF B_y , IMF B_z , and solar-wind dynamic pressure, P_{sw} on the north-south index correlations.

Figure 1.7 shows the magnitude of the AE/SAE and NAE/SAE correlations as a function of IMF B_z and P_{sw} . The IMF and dynamic pressure data accompanying the correlation coefficients are binned at 1 nT and 0.25 nPa bins. In each bin, we plot the percentage of high-correlation coefficients ($R > 0.7$) that occur during the bin conditions. The “percentage of correlations” quantity was chosen over the average bin correlation coefficient because it shows the IMF and dynamic pressure dependence more clearly. It is clear that both the AE/SAE (left) and NAE/SAE (right) plots suggest strong dependence of the north/south correlations on IMF B_z and P_{sw} . The percentage of high coefficients is higher for southward IMF, and for steady IMF it increases with dynamic pressure. In other words, the more southward the IMF and the higher the dynamic pressure, the better correlated the north-south electrojets are, while more northward IMF and low dynamic pressure are more statistically likely to produce asymmetrical north and south electrojets. We should caution here that high correlations between north and south indices do not exclude high differences in amplitude between north and south, and future work will address all these issues. Both IMF B_z and high dynamic pressure can be strong drivers of geomagnetic activity, relocating magnetospheric population boundaries, enhancing large-scale field-aligned currents, enhancing convection in the magnetosphere and ionosphere, as well as ionospheric currents. Under strongly driven conditions, both SAE and NAE (or AE) would be characterized by distinct enhancements well correlated in time,

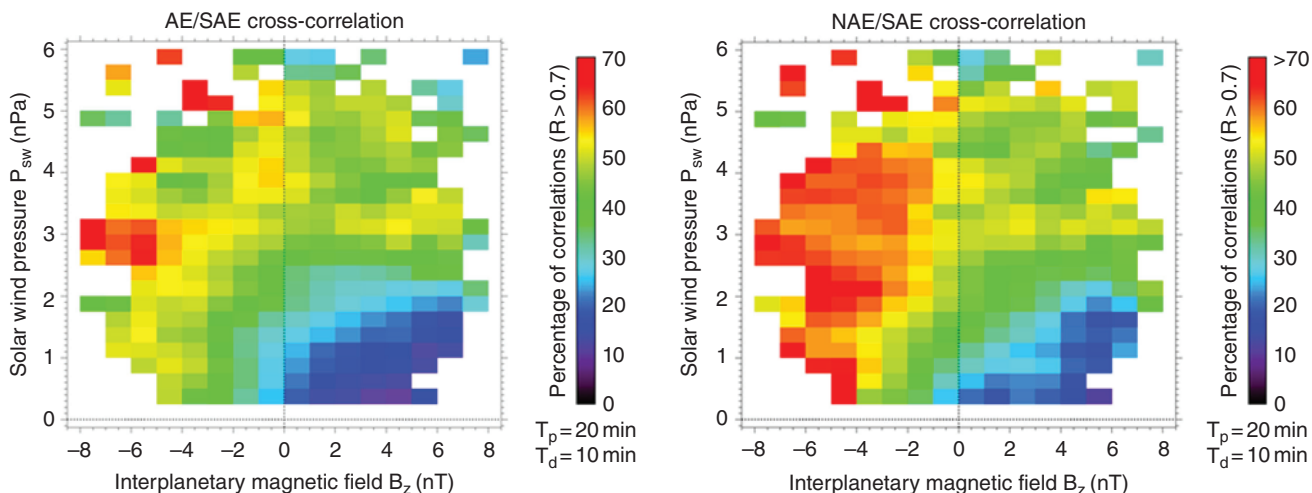


Figure 1.7 (Left) AE/SAE and (right) NAE/SAE correlation results as a function of ACE IMF B_z and solar wind dynamic pressure.

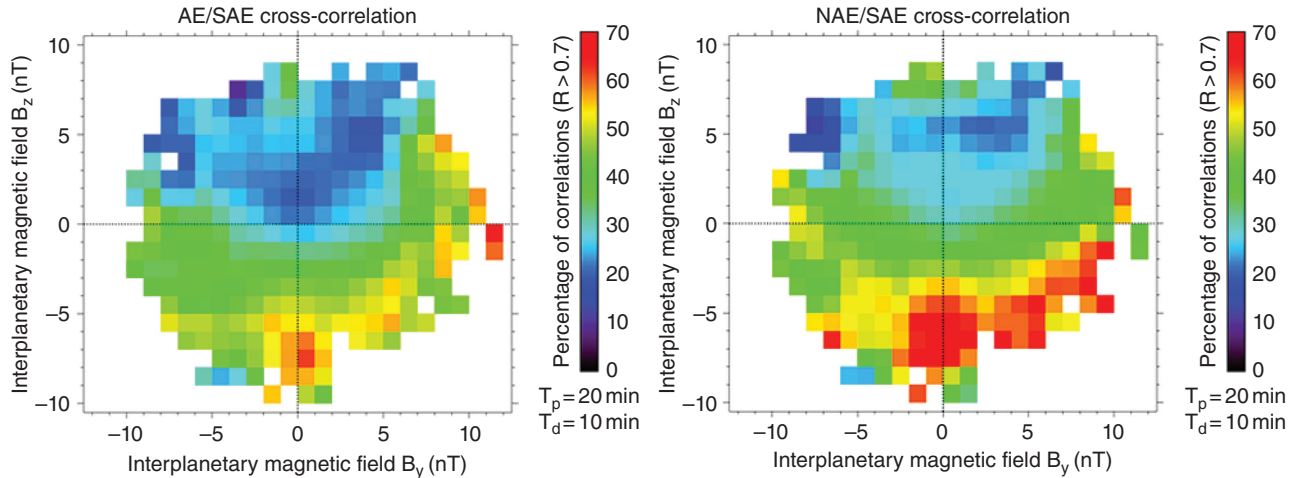


Figure 1.8 (Left) AE/SAE and (right) NAE/SAE correlation results as a function of ACE IMF B_y and B_z .

leading to high correlation coefficients even though their amplitude differences may not be necessarily small.

Figure 1.8 shows the dependence of the percentage of high correlations on the concurrent IMF B_y and B_z components. The IMF B_z dependence is again clear. In addition, high correlation coefficients appear for high absolute values of IMF B_y , even when the IMF is northward. Furthermore, high correlations seem to be present when the IMF is purely northward but with high magnitude; however, it is unclear if this is a real dependence or result of low statistics at these high northward IMF values. An asymmetry for positive and negative IMF B_y is also evident, mostly for southward IMF. We see stronger correlations for positive IMF B_y than for negative IMF B_y .

1.3. ULF WAVE POWER ASYMMETRIES

Ultra low frequency waves are the lowest frequency magnetohydrodynamic (MHD) waves generated in the magnetosphere in response to solar-wind drivers and internal dynamic processes. They are an excellent diagnostic tool that can determine and track the energy flow from the solar wind and through the different magnetospheric regions. They also provide a good way of understanding how magnetospheric processes couple down to the ionosphere and thermosphere. For example, *Yizengaw et al.* [2013] demonstrated that during a solar-wind high speed stream (HSS) event, upstream oscillations directly drove ULF waves globally within the magnetosphere, which also penetrated to the ionosphere at all latitudes and down to the equator where they drove similar oscillation in the equatorial electrojet and the measured ionospheric total electron content (TEC).

1.3.1. Prior Studies

Conjugate studies of ULF waves can additionally provide information on how the flow of energy from the solar wind is distributed to the two hemispheres, but unfortunately such prior studies are few and far between.

Most of the conjugate studies on ULF pulsations have been done at high latitudes and the cusp. *Ables et al.* [2000] and *Liu et al.* [2003] studied resonant Pc5 waves with high conjugacy to determine IMF dependencies, *Matthews et al.* [1996] used both ground magnetometers and radar observations to study the conjugate wave response to a solar-wind shock impact, and *Posch et al.* [1999] looked at conjugate asymmetries of broadband (0–50 mHz) waves.

Conjugate wave studies from lower latitudes are just as uncommon as high-latitude studies. A series of publications looked at various aspects of conjugacy in Pc4-5 waves near $L=4$, using magnetometer data from Siple station in Antarctica and a set of three near conjugate stations from the north. *Lanzerotti et al.* [1973] and *Surkan and Lanzerotti* [1974] looked at the conjugate wave power at quiet and disturbed conditions, respectively, during the 1971 December solstice. They found that during quiet days the ratio of south to north wave power was ~ 1 , but for disturbed days the wave power was much stronger in the southern station, which is opposite to what we are reporting here, but they examined higher latitudes. *Feng et al.* [1995] studied conjugate Pc3-4 pulsations at low latitude, $L=1.2$, and while they did not report on the relative wave power between the north and south stations, they found evidence that the observed waves were due to resonances and their daily occurrence pattern is controlled by their source and propagation characteristics.

Obana et al. [2005] studied the north-south asymmetry of Pc3-5 waves at higher latitudes with a pair of conjugate stations at $L = 5.4$. While the latitude of the conjugate observations is much higher than the low-latitude and midlatitude station pairs we are including in our study, the *Obana et al.* [2005] work is the only other work that directly looks at the wave-power ratio between the two hemispheres. They found a seasonal variation in the north vs. south power ratio and also found that the power in the northern station is always higher than at the southern stations throughout the year, as we report here. They named that the “positive effect.” They considered ionospheric conductivity effects as the source for the observed seasonal asymmetries and differences in the magnitude of the background magnetic field to explain the positive effect. We provide more detailed comparisons in the section below.

1.3.2. Low Latitude and Midlatitude ULF Wave-Power Asymmetries

We performed a conjugate study of ULF wave power along the Americas meridian and we present here some key representative results. We utilized stations from three magnetometer chains: the South American Meridional B-field Array (SAMBA) [Boudouridis and Zesta, 2007], a chain of 12 magnetometers along Chile and in Antarctica, covering mostly low latitudes and midlatitudes, the Magnetometers along the Eastern Atlantic Seaboard for Undergraduate Research and Education (MEASURE) [Berube et al., 2003], which has several stations along the East Coast of the United States, some of them being directly conjugate with SAMBA stations, and the Midcontinent Magnetoseismic Chain (McMAC) [Chi et al., 2013], which extends the CARISMA (Canadian Array for Realtime Investigations of Magnetic Activity) Churchill line of magnetometers southward to Mexico at low latitudes. The McMAC meridian is approximately 2 hr of MLT separated by the average meridian of the MEASURE and SAMBA chains.

Figure 1.9 is a map of the magnetometer locations set in the Southern Hemisphere with the three Northern Hemisphere stations that we used projected to their magnetic conjugate points, using the appropriate epoch IGRF model. The dotted lines are lines of geographic latitude 10° apart, and geographic longitude 20° apart. The blue lines are lines of constant geomagnetic latitude from -10° to -60° . The southern SAMBA stations of PAC, OHI, and PAL are denoted as blue solid circles, while the northern stations of FIT and APL from MEASURE, and AMER from McMAC are red solid circles. FIT and PAC are approximately at $L = 1.7$, while the remaining stations are approximately at $L = 2.3$.

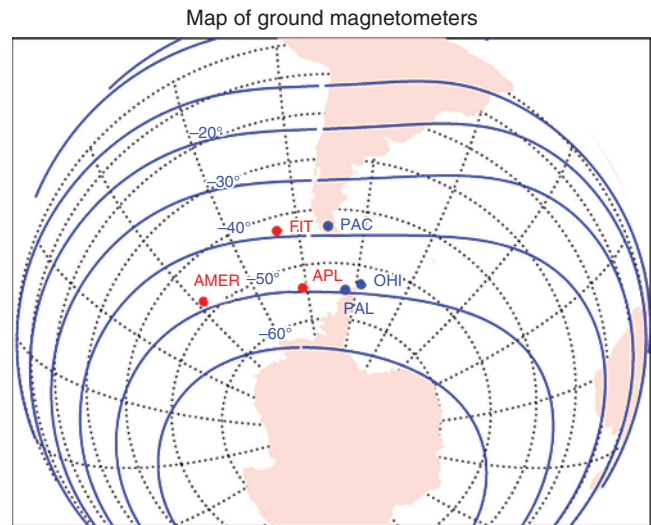


Figure 1.9 Map showing the southern and northern conjugate stations that were used for studying the north-south asymmetries of ULF wave power. In blue are the southern SAMBA stations, while in red are the conjugate projections of the northern MEASURE and McMAC stations.

For our comparisons of interhemispheric wave power and its seasonal and annual variations, we calculate the total daily power separately in the Pc3 (20–100 mHz) and Pc4-5 (2–20 mHz) bands for each station. The daily power calculation includes only the dayside, approximately 0630–1730 MLT, for each station. Pc3–Pc5 waves typically have different sources on the dayside and nightside and are regularly present and stronger on the dayside, resulting primarily from upstream sources and solar wind magnetosphere interactions [e.g., Yumoto, 1985; Troitskaya and Bolshakova, 1988]. Our station pairs are conjugate in latitude but can be separated in MLT by as little as a half hour, in the case of the FIT-PAC pair, or as much as 3 hr, in the case of the AMER-OHI pair. Since this is a statistical study with only daily values of dayside wave power, any instantaneous MLT differences between our conjugate pairs of stations do not influence our conclusions. We calculate the daily total power from the dynamic spectrum analysis from summed 1 min bins. We calculate the total power in all frequency bins every 1 min with a 10-min Fourier window centered on the minute of calculation. We continue moving our 10-min window to the subsequent slot until the full dayside period is covered and the total daily power is the sum of the power values of all the individual 1-min bins. We do this at each station and for the two frequency regimes, Pc3 and Pc4-5.

Figure 1.10 shows the results for the PAC-FIT pair of stations at $L = 1.7$ and for year 2005. The top panel shows the daily power for the north station FIT in red and for the south station PAC in blue. The bottom panel shows the ratio of the north to south station power (FIT-PAC).

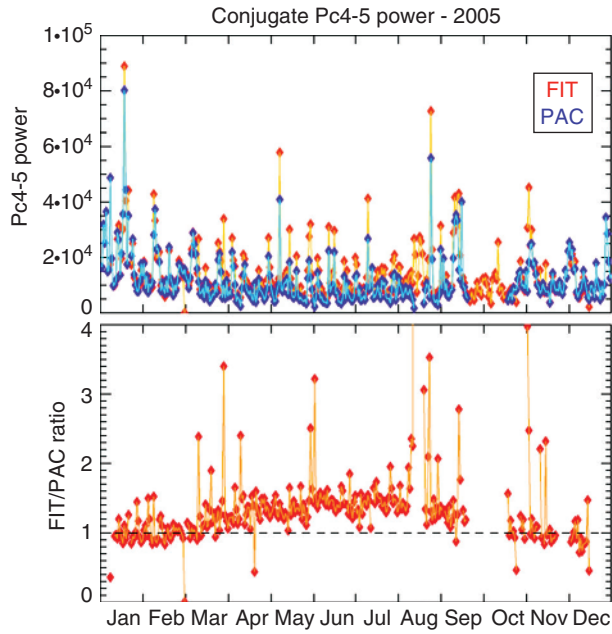


Figure 1.10 Conjugate Pc4-5 power at L = 1.7 for the FIT-PAC pair and for year 2005. The wave power for the north station FIT (red) and south station PAC (blue) is shown in the top panel, while the north-to-south power ratio is shown in the bottom panel.

A clear seasonal/annual variation is seen in the FIT-PAC ratio, with the ratio maximizing at June solstice (more illumination of the Northern Hemisphere) and minimizing at December solstice (less illumination of the Northern Hemisphere), which is intuitively expected by the ionospheric illumination patterns of the north and south hemispheres during the solstices. Most interesting, the December minimum of the FIT-PAC ratio is ~ 1 , indicating similar wave power in the two hemispheres during December solstice, while the ratio maximum is ~ 1.5 , indicating much stronger wave power in the north during June solstice. In short, there seems to be a Northern Hemisphere bias, in addition to the annual seasonal variation of wave power, with the northern station having consistently higher power than the southern station throughout the year.

This pattern observed in Figure 1.10 is consistent for both Pc3 and Pc4-5 bands and at both low-latitude ($L=1.7$) and midlatitude ($L=2.3$) conjugate stations. Figure 1.11 shows the daily Pc4-5 wave-power values for FIT on top and PAC on the bottom for year 2005 with polynomial fitted lines to demonstrate the annual variation of the data. We found that the best fit was a second order polynomial of the form $ax^2 + bx + c$, and it is shown

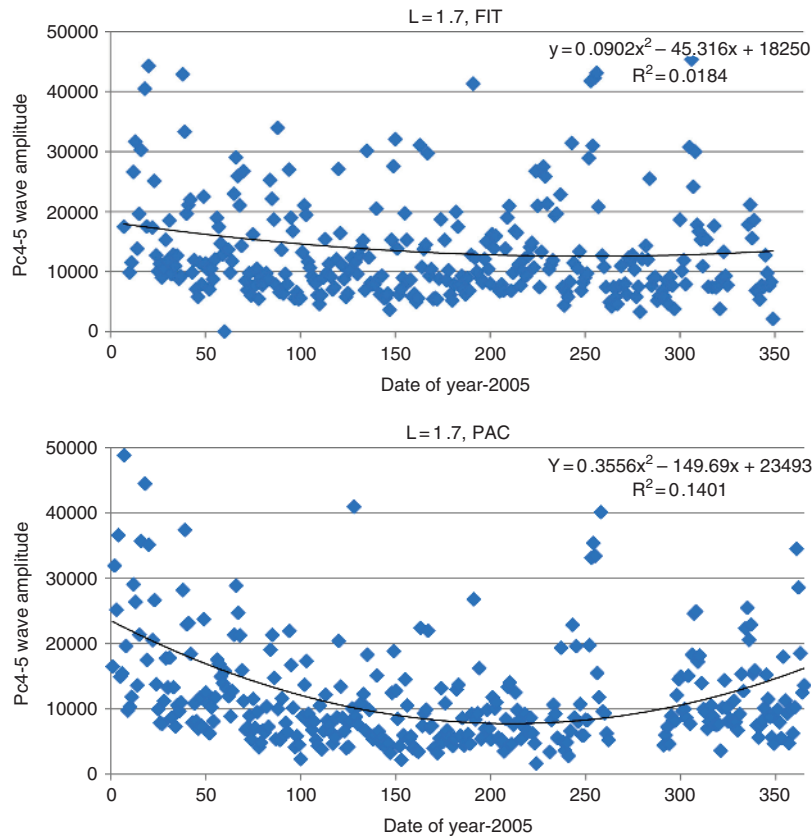


Figure 1.11 Annual distribution of the FIT and PAC daily wave power for 2005 and with second-order polynomial fits to demonstrate any seasonal trends.

as a solid black line with the equation and R^2 value on the figure. While the R^2 is poor for both stations, it does seem to fit well the general shape of the bulk of points in each panel. Our results then are indicative of the situation of the two hemispheres during periods of lower to moderate geomagnetic activity. The northern line fit is rather flat, while the southern line fit has a clear curvature with high amplitudes around the December solstice. PAC has a higher a coefficient value, which leads to the curved shape and R^2 values demonstrating a stronger correlation. The shape of this regression line is a driver for the shape of the power ratio plots seen in Figure 1.10. It is the south decreasing around the June solstice and not the north increasing that drives the shape of the power ratio. Second, the northern station line is shifted up throughout the year, which causes the power ratio to remain above 1. The interesting conclusion from this analysis seems to be that the northern station exhibits only very weak annual or seasonal variation (if at all) while the southern station shows significant seasonal variation, which in turn determines the ratio of the north-south ratio.

Our result of a power ratio above 1 for all seasons is in agreement with *Obana et al.* [2005] but the explanation is not. *Obana et al.* explain the “positive effect” as a result of the stronger background magnetic field in the Northern Hemisphere with respect to that in the Southern Hemisphere. This explanation is consistent with the background fields for the conjugate pair FIT-PAC at $L=1.7$. However, the background fields at our conjugate pair at $L=2.3$, AMER-OHI, are similar, and there is still a north-to-south ratio greater than 1 for all seasons. We believe that our explanation outlined in Figure 1.11 better describes all our observations, since the annual wave-power trends for AMER and OHI are very similar to those shown in Figure 1.11.

1.3.3. The Role of the Ionosphere and Thermosphere

Ground magnetometer perturbations are an integrated response to all currents within the sensor’s field of view (typically of radius equal to the distance of the current that impacts the magnetometer, ~ 120 km for ionospheric currents). Inhomogeneous ionospheric conductivity can modulate and influence the characteristics of ULF waves as they are coupled from the magnetosphere down to the ionosphere [*Hughes and Southwood*, 1976; *Pilipenko et al.*, 2000; *Alperovic and Fedorov*, 2007]. The assumption is that the wave electric field will map similarly to both ionospheric footpoints and the resulting field will be a combination of reflected and absorbed components, which depend strongly on the local height-integrated ionospheric conductivity. While it is true that the amount of wave power that penetrates the ionosphere and the amount reflected depend on the conductivity and the Hall to Pedersen ratio, ground magnetometers remotely respond primarily to Hall currents. For the same wave E field, you

get more fluctuation currents, and therefore higher ground perturbations, when you have higher integrated conductivity. Therefore, one would intuitively expect stronger wave power in the more illuminated ionosphere. The variations we show in Figure 1.11 are consistent with this interpretation when considering the geographic latitude of FIT and PAC. FIT is at geographic latitude of 28° and remains well illuminated throughout the year, therefore not exhibiting strong seasonal variation. PAC, on the other hand, is at geographic latitude of -53.2° and shows higher wave power around December solstice, when its ionosphere is better illuminated. *Obana et al.* [2005] looked at the Pc3-5 north-to-south wave-power ratios at $L=5.4$. They found, in agreement with our results, that the Northern Hemisphere has stronger power throughout the year. However, in contrast with our results, they found that the seasonal variation of the power ratio has a peak in December solstice and minimum at June solstice. They suggest that the higher northern conductivity during June solstice actually blocks the transmission of MHD waves from the magnetosphere to ionosphere. This is clearly not true for our conjugate pairs at $L=1.7$, where the power ratio peaks in June and has a minimum in December-January.

We, therefore, examine measurements of the total electron content (TEC), as measured by ground GPS receivers at the two conjugate locations, to examine whether a similar asymmetry pattern as that seen in the wave power is also observed in the ionospheric content. The TEC observed on the ground is dominated by the ionospheric electron density (the plasmaspheric density being significantly smaller) and is therefore a reasonable proxy of the ionospheric content and conductivity at that location. We used data from GPS receivers co-located or in close proximity with our magnetometer stations.

Figure 1.12 shows, in the top panel, the TEC of the north (red) and south (blue) GPS receivers close to the locations of the FIT and PAC magnetometer stations. The ratio of the northern to southern TEC is plotted in the bottom panel for the year 2003. The northern station shows unambiguously higher TEC throughout the year and the north-south ratio remains above 1.0 similar to the Pc4-5 wave-power ratio in Figure 1.10. In contrast to the wave-power ratio, the TEC ratio exhibits a semiannual variation with peaks at the two solstices and dips at the two equinoxes. It is interesting that the absolute TECs at both northern and southern GPS stations has the opposite semiannual variation, namely they peak at the equinoxes and dip at the solstices. In other words, while there is more ionosphere at both hemispheres during equinoxes, the conductivity is more equitably distributed in the two hemispheres. During the solstices, the ionosphere is thinner at both hemispheres in comparison with their respective equinox content, but the Northern Hemisphere has significantly more content irrespective of whether it is the June or December solstice.

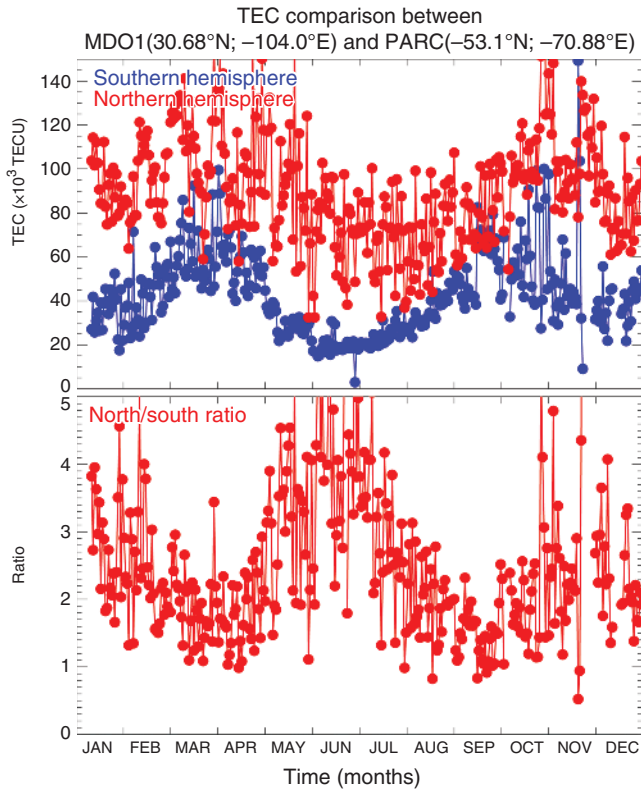


Figure 1.12 (Top panel) Annual distribution of daily TEC at conjugate locations at $L = 1.7$, close to the FIT and PAC magnetometer sites; (bottom panel) the north to south TEC ratio.

This semiannual TEC variation has been reported before by *Lee et al.* [2010] and *Bagiya et al.* [2009], who used individual GPS receivers in Taiwan and India, respectively, to study the diurnal and seasonal variation of TEC at low latitudes. Both studies found a clear semi-annual variation in TEC with peaks at the equinoxes, in exact agreement with our results. It has also been recently reported and examined as global TEC climatology by *Liu et al.* [2009] and *Lean et al.* [2011]. The north-south asymmetries of TEC were examined by *Mendillo et al.* [2005] in terms of global asymmetries. Their Figure 2 clearly shows the north to south asymmetric pattern at low latitudes and midlatitudes in agreement with our observation. We offer, for the first time, similar north to south asymmetries for both ULF wave power and TEC and suggest a link between the two.

Figure 1.13 shows in each column from top to bottom the north-to-south wave-power ratio for Pc3 waves, for Pc4-5 waves, and the TEC north-to-south ratio for years 2006 (left) and 2007 (right) at $L = 2.3$ for the station pair AMER-OHI. Similar to the results at $L = 1.7$ (Fig. 1.10), here we again see a clear seasonal variation in the Pc3 and Pc4-5 ratios, which peaks in northern summer and minimizes in northern winter. The ratio never drops below 1 throughout the year for either frequency band, indicating that there is a strong offset toward the Northern Hemisphere and a systematic asymmetry in addition to the seasonal variation. The offset is stronger for the

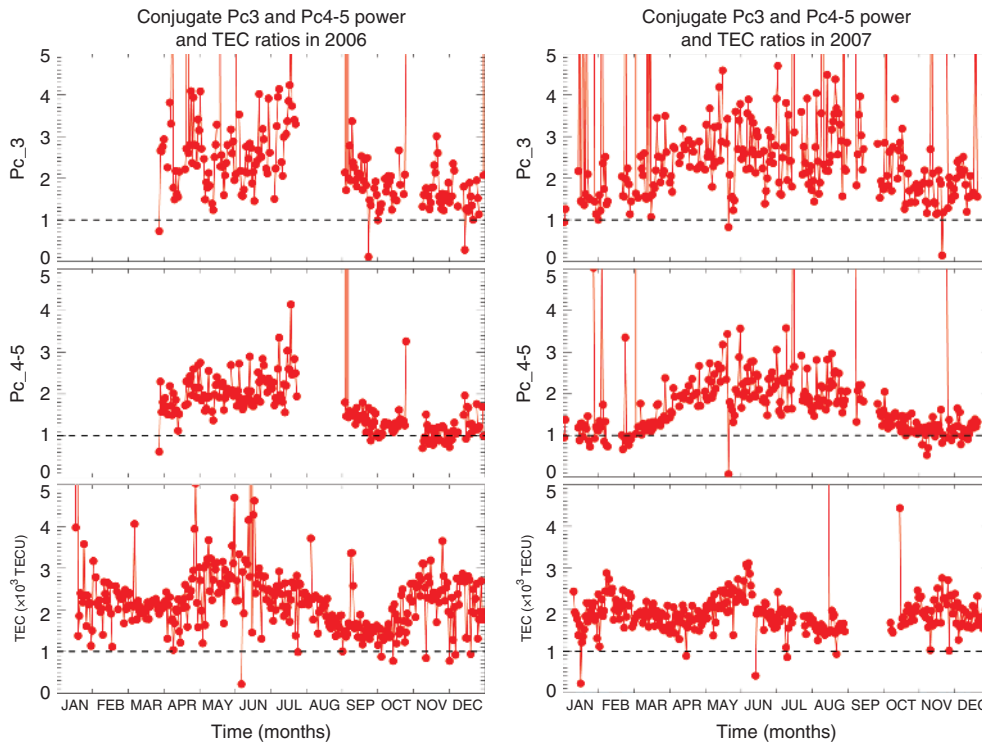


Figure 1.13 From top to bottom, north to south power ratio for Pc3 waves, Pc4-5 waves, and for TEC, at $L = 2.3$ for years 2006 (left) and 2007 (right).

higher frequency waves (for Pc3). The TEC ratio also shows a clear bias toward the Northern Hemisphere (ratio >1 throughout the year), and it is even stronger than the one exhibited by the waves. In addition to the northern bias, the TEC ratio exhibits a clear semiannual variation that peaks at the two solstices and minimizes at the equinoxes.

Note that the annual variation of the waves and the semiannual variation of TEC is much more pronounced at the midlatitude $L = 2.3$, than it was at low latitude of $L = 1.7$ (compare Figs. 1.13 and 1.10). Furthermore, our results only partly agree with the results of *Obana et al.* [2005], who conducted a similar study but at a higher latitude of $L = 5.4$. Although *Obana et al.* [2005] found a similar northern bias in their analysis (their north-to-south power ratio was also always >1), the seasonal variation at their latitude was exactly opposite to the one we report in Figures 1.9 and 1.10. Specifically, they found that the wave-power ratio maximized at northern winter and minimized at northern summer. *Obana et al.* [2005] interpreted their observed seasonal variation as a likely result from inductive shielding of the waves by a highly conducting ionosphere: lower wave power in the summer beneath the higher conductive ionosphere than at winter, according to the shielding theory by *Yoshiwaka et al.* [2002]. However, the results shown in *Obana et al.* [2005] show seasonal variation on the ratio of the north-to-south amplitudes not on the north or south amplitudes themselves, so without knowing the seasonal variation of the wave amplitudes themselves, it is unclear how the inductive shielding theory of *Yoshiwaka et al.* [2002] would apply. In our dataset, there is no clear evidence for ionospheric shielding either, although more detailed analysis will be in a future work.

Perhaps the most intriguing result is the consistent northern bias that we found in both low latitudes and midlatitudes in the Americas meridian, that *Obana et al.* [2005] also found in the Asian meridian, and that the bias is even stronger in the TEC than it is in the ULF wave power. There are similar results in *Titheridge and Buonsanto* [1983] and *Su et al.* [1998] who both studied the annual variations of the low-latitude topside ionosphere from satellite and ground observations. Both of the *Titheridge and Buonsanto* [1983] and *Su et al.* [1998] studies found that the TEC and topside density values, respectively, are higher during the December solstice than during the June solstice, and they were able to show that the chemistry and dynamics of the neutral species have a significant effect in shaping the observed asymmetries.

Titheridge and Buonsanto [1983] looked at TEC from two near-conjugate pairs of ground stations for a period of 3 yr and also found a persistent higher amplitude of TEC in the Northern Hemisphere than in the Southern Hemisphere. *Su et al.* [1998] used observations from the

low-inclination Hinotori satellite to look primarily at longitudinal patterns of the electron density, but also saw similar north-south TEC asymmetries, which they attributed to neutral winds. While they were not able to explain this, both studies suggested some type of trans-equatorial neutral wind could be the cause of the asymmetries. We suggest that there is potentially a strong connection between neutral, plasma, and wave properties. Future work should clarify whether such north-south asymmetries occur at all longitudes and latitudes and illuminate their physical sources.

In summary, the ULF wave power shows a clear inter-hemispheric asymmetry with stronger power always in the northern conjugate station. This north-south asymmetry is stronger at midlatitudes than at low latitudes (higher ratios at $L = 2.3$ than at $L = 1.7$) and it is stronger for the higher frequency waves (higher ratios for Pc3 waves). The ionospheric TEC exhibits the same inter-hemispheric asymmetry, implying that the state of the ionosphere affects and partly causes the observed wave interhemispheric asymmetry. It is unclear why the TEC ratio has a biannual variation while the wave power only exhibits annual variation and needs to be further investigated in future work.

1.4. SUMMARY

We explore pathways for energy input into the ionosphere-thermosphere system and asymmetries between the Northern and Southern Hemispheres. Seasonal effects are strong drivers of interhemispheric asymmetries, the uneven illumination of the two hemispheres resulting in asymmetric ionospheric conductivities and therefore asymmetric current distribution in the two hemispheres. Additional factors may also contribute significantly to the asymmetric energy input into the two hemispheres as prior studies have reported. Factors like the Earth's dipole tilt with respect to the rotation axis, the IMF orientation, local magnetic field structures, and even atmospheric dynamics. We review several of these factors and their effects. We focus on asymmetries of auroral dynamics, particularly substorms, for which there is considerable prior work defining their onset and dynamics in the two hemispheres. Similar asymmetries should be expected in the auroral electrojets that are well correlated with the auroral dynamics.

We calculate a Southern Hemisphere auroral electrojet index, SAE, from all available southern auroral stations and compare it with a conjugate northern auroral electrojet index, NAE, and with the standard AE index. We look at both case studies and a large statistical study of the correlations and difference between SAE, NAE, and AE. We found that, in general, SAE correlates well with AE and even better with NAE and that correlation is better under strong southward IMF and/or strong solar-wind dynamic

pressure. Strong interhemispheric asymmetries occur often and are likely the result of IMF B_y or interhemispheric currents. Differences in the amplitude of the electrojet indices between the two hemispheres are strongest in the local midnight and are the result of the nightside westward electrojet.

We look at the power of ULF waves in two bands, Pc3 (20–100 mHz), and Pc4-5 (2–20 mHz) and study the power in pairs of conjugate stations at low latitudes, L=1.7, and midlatitudes, L=2.3, in the Americas meridian. We calculate the daily wave power in the two frequency bands and then calculate the north-to-south daily power ratio. We find that the ULF wave power shows a clear interhemispheric asymmetry with stronger power always in the northern conjugate station. This north-south asymmetry is stronger at midlatitudes than at low latitudes (higher ratios at L=2.3 than at L=1.7), and it is stronger for the higher frequency waves (higher ratios for Pc3 waves). The ionospheric TEC exhibits similar interhemispheric asymmetry, namely higher TEC all year round in the Northern Hemisphere, implying that the state of the ionosphere affects and partly causes the observed wave interhemispheric asymmetry. We believe that the link between the ULF wave power and TEC are in the north-south asymmetry, but the seasonal-annual variation of the ULF power and TEC are different and the result of different processes.

ACKNOWLEDGMENTS

This work was supported by NSF grant ATM-0100902, NSF grant OPP-ANT-1043621, AFOSR grant LRIR #10RV07COR, NASA LWS (NNX10AQ53G) and Geospace Science programs (NNX07AM22G and NNX09AR84G), and AFOSR YIP grant (FA9550-10-1-0096). We would also like to thank GIMA (Geophysical Institute Magnetometer Array) for the data from the BET station; the THEMIS team for the data from SNKQ and KIAN; DMI (Danish Meteorological Institute) for data from AMK, NAQ, and SCO; BAS (British Antarctic Survey) for data from the HBA and M78-337 stations; Science Institute, University of Iceland, for the data from LVR; Geoscience Australia for data from MCQ and MAW; INTERMAGNET (International Real-time Magnetic Observatory) for data from PBQ; Oleg Troshichev for the data from NVL station; Pieter Stoker for data from the SNA magnetometer; IMAGE (International Monitor for Auroral Geomagnetic Effects) for the data from SOR and BJN; the WDC for Aurora in National Institute of Polar Research in Japan for data from the HLL and SYO stations; and the WDC for geomagnetism, Kyoto, for the standard AE index data.

REFERENCES

- Ables, S. T., B. J. Fraser, J. V. Olson, and R. J. Morris (2000), Conjugate ULF field line resonances at cusp latitudes, *Advances in Space Res.*, 26(1), 125–130; ISSN 0273-1177; [http://dx.doi.org/10.1016/S0273-1177\(99\)01038-8](http://dx.doi.org/10.1016/S0273-1177(99)01038-8).
- Alperovich, L. S., and E. N. Fedorov (2007), *Hydromagnetic Waves in the Magnetosphere and the Ionosphere*, vol. 353, Astrophysics and Space Science Library, XXIV.
- Anderson, B. J., K. Takahashi, T. Kamei, C. L. Waters, and B. A. Toth (2002), Birkeland current system key parameters derived from Iridium observations: Method and initial validation results, *J. Geophys. Res.*, 107(A6); doi:10.1029/2001JA000080.
- Bagiya, M. S., H. P. Joshi, K. N. Iyer, M. Aggarwal, S. Ravindram, and B. M. Pathan (2009), TEC variations during low solar activity period (2005–2007) near the Equatorial Ionospheric Anomaly Crest region in India, *Ann. Geophysicae*, 27, 1047–1057; doi:10.5194/angeo-27-1047-2009.
- Baker, K. B., and S. Wing (1989), A new magnetic coordinate system for conjugate studies at high latitudes, *J. Geophys. Res.*, 94(A7), 9139–9143; doi:10.1029/JA094iA07p09139.
- Belon, A. E., J. E. Maggs, T. N. Davis, K. B. Mather, N. W. Glass, and G. F. Hughes (1969), Conjugacy of visual auroras during magnetically quiet periods, *J. Geophys. Res.*, 74, 1–28; doi:10.1029/JA074i001p00001.
- Benkevich, L., W. Lyatsky, and L. L. Cogger (2000), Field-aligned currents between the conjugate hemispheres, *J. Geophys. Res.*, 105, 27727–27737; doi:10.1029/2000JA900095.
- Berube, D., M. B. Moldwin, and J. M. Weygand (2003), An automated method for the detection of field line resonance frequencies using ground magnetometer techniques, *J. Geophys. Res.*, 108, 1348; doi:10.1029/2002JA009737, A9.
- Boudouridis, A., and E. Zesta (2007), Comparison of Fourier and wavelet techniques in the determination of geomagnetic field line resonances, *J. Geophys. Res.*, 112, A08205; doi:10.1029/2006JA011922.
- Chi, P. J., et al. (2013), Sounding of the plasmasphere by Mid-continent Magnetoseismic Chain (McMAC) magnetometers, *J. Geophys. Res. Space Phys.*, 118, 3077–3086; doi:10.1002/jgra.50274.
- Cnossen, I., and A. D. Richmond (2012), How changes in the tilt angle of the geomagnetic dipole affect the coupled magnetosphere-ionosphere-thermosphere system, *J. Geophys. Res.*, 117, A10317; doi:10.1029/2012JA018056.
- Davis, T. N., and M. Sugiura (1966), Auroral electrojet index AE and its universal time variations, *J. Geophys. Res.*, 71, 785–801.
- Feng, Q., B. J. Fraser, F. W. Menk, C. W. S. Ziesolleck, O. Saka, and T. Kitamura (1995), Pc3-4 geomagnetic pulsations observed at very low latitude conjugate stations, *J. Geophys. Res.*, 100(A10), 19287–19298; doi:10.1029/94JA01260.
- Fillingim, M. O., G. K. Parks, H. U. Frey, T. J. Immel, and S. B. Mende (2005), Hemispheric asymmetry of the after-noon electron aurora, *Geophys. Res. Lett.*, 32, L03113; doi:10.1029/2004GL021635.
- Förster, M., and I. Cnossen (2013), Upper atmosphere differences between northern and southern high latitudes: The role of magnetic field asymmetry, *J. Geophys. Res. Space Phys.*, 118, 5951–5966; doi:10.1002/jgra.50554.

- Frank, L. A., and J. B. Sigwarth (2003), Simultaneous images of the northern and southern auroras from the polar spacecraft: An auroral substorm, *J. Geophys. Res.*, *108*, 8015; doi:10.1029/2002JA009356.
- Gjerloev, J. W. (2012), The SuperMAG data processing technique, *J. Geophys. Res.*, *117*, A09213; doi:10.1029/2012JA017683.
- Hajkovicz, L. A. (2006), Magnetoconjugate phenomena in Alaska and Macquarie Is., Australia in 2003: Position of the global maximum iso-aurorae, *Ann. Geophysicae*, *24*, 2611–2617; doi:10.5194/angeo-24-2611-2006.
- Hughes, W. J., and D. J. Southwood (1976), An illustration of modification of geomagnetic pulsation structure by the ionosphere, *J. Geophys. Res.*, *81*, 3241–3247; doi:10.1029/JA081i019p03241.
- Kivelson, M. G., K. K. Khurana, R. J. Walker, L. Kepko, and D. Xu (1996), Flux ropes, interhemispheric conjugacy, and magnetospheric current closure, *J. Geophys. Res.*, *101*, 27,341–27,350; doi:10.1029/96JA02220.
- Knipp, D. J., C.-H. Lin, B. A. Emery, J. M. Ruohoniemi, F. J. Rich, and D. S. Evans (2000), Hemispheric asymmetries in ionospheric electrodynamics during the solar wind void of 11 May 1999, *Geophys. Res. Lett.*, *27*, 4013; doi:10.1029/2000GL003801.
- Lanzerotti, L. J., and M. F. Robbins (1973), ULF geomagnetic power near $L = 4$: 1. Quiet day power spectra at conjugate points during December Solstice, *J. Geophys. Res.*, *78*(19), 3816–3827; doi:10.1029/JA078i019p03816.
- Laundal, K. M., and N. Ostgaard (2009), Asymmetric auroral intensities in the Earth's Northern and Southern hemispheres, *Nature*, *460*, 491–493; doi:10.1038/nature08154.
- Lean, J. L., R. R. Meier, J. M. Picone, and J. T. Emmert (2011), Ionospheric total electron content: Global and hemispheric climatology, *J. Geophys. Res.*, *116*, A10318; doi:10.1029/2011JA016567.
- Lee, C. C., Y. J. Chuo, F. D. Chu (2010), Climatology of total electron content near the dip equator under geomagnetic quiet-conditions, *J. Atmos. Solar Terr. Phys.*, *72*(2–3), February, 207–212; <http://dx.doi.org/10.1016/j.jastp.2009.11.011>.
- Liou, K., P. T. Newell, C.-I. Meng, M. Brittnacher, and G. Parks (2001), Seasonal effects on auroral particle acceleration and precipitation, *J. Geophys. Res.*, *106*, 5531–5542; doi:10.1029/1999JA000391.
- Liu, L., W. Wan, B. Ning, and M.-L. Zhang (2009), Climatology of the mean total electron content derived from GPS global ionospheric maps, *J. Geophys. Res.*, *114*, A0630; doi:10.1029/2009JA014244.
- Liu, Y. H., B. J. Fraser, R. Y. Liu, and P. V. Ponomarenko (2003), Conjugate phase studies of ULF waves in the Pc5 band near the cusp, *J. Geophys. Res.*, *108*, 1274; doi:10.1029/2002JA009336.
- Lyatskaya, S., W. Lyatsky, and G. V. Khazanov (2014a), Effect of interhemispheric field-aligned currents on the Region 1 currents, *Geophys. Res. Lett.*, *41*, 3731–3737; doi:10.1002/2014GL060413.
- Lyatskaya, S., G. V. Khazanov, and E. Zesta (2014b), Interhemispheric field-aligned currents: Simulation results, *J. Geophys. Res.*; doi:10.1002/2013JA019558.
- MacLennan, C. G., L. J. Lanzerotti, S. -I. Akasofu, A. N. Zaitzev, P. J. Wilkinson, A. Wolfe, and V. Popov (1991), Comparison of “electrojet” indices from the Northern and Southern hemispheres, *J. Geophys. Res.*, *96*, 267–264; doi:10.1029/90JA01366.
- Mendillo, M., C.-L. Huang, X. Pi, H. Rishbeth, R. Meier (2005), The global ionospheric asymmetry in total electron content, *J. Atmos. Solar Terr. Phys.*, *67*(15), 1377–1387; <http://dx.doi.org/10.1016/j.jastp.2005.06.021>.
- Morioka, A., et al. (2011), On the simultaneity of substorm onset between two hemispheres, *J. Geophys. Res.*, *116*, A04211; doi:10.1029/2010JA016174.
- Matthews, D. L., J. M. Ruohoniemi, J. R. Dudeney, C. F. Farrugia, L. J. Lanzerotti, and E. Friis-Christensen (1996), Conjugate cusp-region ULF pulsation responses to the solar wind event of 23 May 1989, *J. Geophys. Res.*, *101*(A4), 7829–7841; doi:10.1029/95JA03470.
- Motoba T., K. Hosokawa, A. Kadokura, and N. Sato, Magnetic conjugacy of northern and southern auroral beads, *Geophys. Res. Lett.*, *39*, L08108; doi:10.1029/2012GL051599, 2012.
- Motoba, T., K. Hosokawa, N. Sato, A. Kadokura, and G. Bjornsson (2010), Varying interplanetary magnetic field By effects on interhemispheric conjugate auroral features during a weak substorm, *J. Geophys. Res.*, *115*, A09210; doi:10.1029/2010JA015369.
- Motoba, T., S. Ohtani, A. Kadokura, and J. Gjerloev (2014), Interrelationship between preonset auroral and magnetic signatures at a geomagnetically conjugate Iceland-Syowa pair, *J. Geophys. Res. Space Phys.*, *119*; doi:10.1002/2013JA019512.
- Newell, P. T., C.-I. Meng, and K. M. Lyons (1996), Suppression of discrete aurorae by sunlight, *Nature* *381*, 766–767; doi:10.1038/381766a0.
- Nishida, A. (1968), Geomagnetic DP-2 fluctuations and associated magnetospheric phenomena, *J. Geophys. Res.*, *13*, 1795; doi:10.1029/JA073i005p01795.
- Obana, Y., A. Yoshikawa, J. V. Olson, R. J. Morris, B. J. Fraser, and K. Yumoto (2005), North-south asymmetry of the amplitude of high-latitude Pc3-5 pulsations: Observations at conjugate stations, *J. Geophys. Res.*, *110*, A10214; doi:10.1029/2003JA010242.
- Østgaard, N., N. A. Tsyganenko, S. B. Mende, H. U. Frey, T. J. Immel, M. Fillingim, L. A. Frank, and J. B. Sigwarth (2005), Observations and model predictions of substorm auroral asymmetries in the conjugate hemispheres, *Geophys. Res. Lett.*, *32*, L05111; doi:10.1029/2004GL022166.
- Østgaard, N., S. B. Mende, H. U. Frey, J. B. Sigwarth, A. Åsnes, J. M. Weygand (2007), Auroral conjugacy studies based on global imaging, *J. Atmos. Solar Terr. Phys.*, *69*, 249–255; doi:10.1016/j.jastp.2006.05.026.
- Østgaard, N., S. B. Mende, H. U. Frey, T. J. Immel, L. A. Frank, J. B. Sigwarth, T. J. Stubbs (2004), Interplanetary magnetic field control of the location of substorm onset and auroral features in the conjugate hemisphere, *J. Geophys. Res.*, *109*, A07204; doi:10.1029/2003J010370.
- Pilipenko, V., M. Vellante, and E. Fedorov (2000), Distortion of the ULF wave spatial structure upon transmission through the ionosphere, *J. Geophys. Res.*, *105*, 21225–21236; doi:10.1029/2000JA900063.
- Posch, J. L., M. J. Engebretson, A. T. Weatherwax, D. L. Detrick, W. J. Hughes, and C. G. MacLennan (1999), Characteristics of broadband ULF magnetic pulsations at conjugate cusp latitude stations, *J. Geophys. Res.*, *104*(A1), 311–331; doi:10.1029/98JA02722.
- Saroso, S. M. Sugiura, T. Iyemori, T. Araki, and T. Kamei (1992), Derivation of polar cap AE indices, *Proc. NIPR Symp. Upper Atmos. Phys.*, *5*, 35–45.

- Sato, N., A. Kadokura, T. Motoba, K. Hosokawa, G. Björnsson, and T. Saemundsson (2012), Ground-based aurora conjugacy and dynamic tracing of geomagnetic conjugate points, 91–98, in *Auroral Phenomenology and Magnetospheric Processes: Earth and Other Planets*, AGU Geophys. Monogr. Ser., vol. 197, edited by A. Keiling et al., Washington, DC: doi:10.1029/2011GM001154, 2012.
- Sato, N., T. Nagaoka, K. Hashimoto, and T. Saemundsson (1998), Conjugacy of isolated auroral arcs and nonconjugate auroral breakups, *J. Geophys. Res.*, *103*, 11,641–11,652; doi:10.1029/98JA00461.
- Shi, J., J. Guo, M. Dunlop, M., T. Zhang, Z. Liu, E. Lucek, A. Fazakerley, H. Rème, and I. Dandouras (2012), Inter-hemispheric asymmetry of dependence of the cusp location on dipole tilt during northward IMF conditions, *Ann. Geophys.*, *30*, 21–26; doi:10.5194/angeo-30-21-2012.
- Stenbaek-Nielsen, H. C., T. N. Davis, and N. W. Glass (1972), Relative motion of auroral conjugate points during substorms, *J. Geophys. Res.*, *77*, 1844–1858; doi:10.1029/JA077i010p01844.
- Stenbaek-Nielsen, H. C., T. N. Wescott, T. N., Davis, and R. W. Peterson (1973), Auroral intensity differences at conjugate points, *J. Geophys. Res.*, *78*, 659–671; doi:10.1029/JA078i004p00659.
- Stubbs, T. J., R. R. Vondrak, N. Østgaard, J. B. Sigwarth, and L. A. Frank (2005), Simultaneous observations of the auroral oval in both hemispheres under varying conditions, *Geophys. Res. Lett.*, *32*, L03103; doi:10.1029/2004GL021199.
- Su, Y. Z., G. J. Bailey, and K. -I. Oyama (1998), Annual and seasonal variations in the low-latitude topside ionosphere, *Ann. Geophysicae*, *16*(8), 974–985; doi:10.1007/s00585-998-0974-0.
- Surkan, A. J., and L. J. Lanzerotti (1974), ULF geomagnetic power near $L = 4.3$. Statistical study of power spectra in conjugate areas during December solstice, *J. Geophys. Res.*, *79*(16), 2403–2412; doi:10.1029/JA079i016p02403.
- Titheridge, J. E., and M. J. Buonsanto (1983), Annual variations in the electron content and height of the F layer in the Northern and Southern hemispheres, related to neutral composition, *J. Atmos. Solar Terr. Phys.*, *45*(10), 683–696; http://dx.doi.org/10.1016/S0021-9169(83)80027-0.
- Troitskaya, V. A., and O. V. Bolshakova (1988), Diagnostics of the magnetosphere using multipoint measurements of ULF-waves, *Advances in Space Res.*, *8*(9–10), 413–425; http://dx.doi.org/10.1016/0273-1177(88)90155-X.
- Weimer, D. R. (2004), Correction to “Predicting interplanetary magnetic field (IMF) propagation delay times using the minimum variance technique,” *J. Geophys. Res.*, *109*, A12104; doi:10.1029/2004JA010691.
- Weimer, D. R., D. M. Ober, N. C. Maynard, M. R. Collier, D. J. McComas, N. F. Ness, C. W. Smith, and J. Watermann (2003), Predicting interplanetary magnetic field (IMF) propagation delay times using the minimum variance technique, *J. Geophys. Res.*, *108*, 1026; doi:10.1029/2002JA009405.
- Weygand, J. M., and E. Zesta (2008), Comparison of auroral electrojet indices in the Northern and Southern hemispheres, *J. Geophys. Res.*, *113*, A08202; doi:10.1029/2008JA013055.
- Weygand, J. M., E. Zesta, and O. Troshichev (2014a), Auroral electrojet indices in the Northern and Southern hemispheres: A statistical comparison, *J. Geophys. Res. Space Phys.*, *119*, 4819–4840; doi:10.1002/2013JA019377.
- Weygand, J. M., E. Zesta, R. L. McPherron, and T. -S. Hsu (2014), *The Differences in Onset Time of Conjugate Substorms, the American Geophysical Union Fall Conference*, San Francisco, CA, December 2014, *EOS Trans.*, *95*, 2014b.
- Wu, Q., T. J. Rosenberg, L. J. Lanzerotti, C. G. MacLennan, and A. Wolfe (1991), Seasonal and diurnal variations of the latitude of the westward auroral electrojet in the nightside polar cap, *J. Geophys. Res.*, *96*(A2), 1409–1419; doi:10.1029/90JA02379.
- Yizengaw, E., E. Zesta, C. M. Biouele, M. B. Moldwin, A. Boudouridis, B. Dantie, A. Mebrahtu, F. Anad, R. F. Pfaff, and M. Hartinger (2013), Observations of ULF wave related equatorial electrojet and density fluctuations, *J. Atmos. Solar Terr. Phys.*; doi:10.1016/j.jastp.2013.03.015.
- Yoshikawa, A., Y. Obana, M. Shinohara, M. Itonaga, and K. Yumoto (2002), Hall-induced inductive shielding effect on magnetic pulsations, *Geophys. Res. Lett.*, *29*(8), 1266; doi:10.1029/2001GL013610.
- Yumoto, K. (1985), Low-frequency upstream wave as a probable source of low-latitude Pc3-4 magnetic pulsations, *Planet. Space Sci.*, *33*(2), 239–249; doi:10.1016/0032-0633(85)90133-3.